N73 25829

N73-25829

NASA TECHNICAL MEMORANDUM

NASA TM X-2773

NASA TM X-2773

CASE FILE COPY

LOW-SPEED WIND-TUNNEL INVESTIGATION OF THE AERODYNAMIC AND ACOUSTIC PERFORMANCE OF A TRANSLATING-CENTERBODY CHOKED-FLOW INLET

by Brent A. Miller and John M. Abbott

Lewis Research Center
Cleveland, Ohio 44135

NATIONAL AERONAUTICS AND SPACE ADMINISTRATION • WASHINGTON, D. C. • JUNE 1973

1. Report No. NASA TM X-2773	2. Government Accession No.	3. Recipient's Catalog No.
4. Title and Subtitle LOW-SPEED WIND-TUNNEL INVESTIGATION OF THE AERODYNAMIC AND ACOUSTIC PERFORMANCE OF A TRANSLATING-CENTERBODY CHOKED-FLOW INLET		5. Report Date June 1973
		6. Performing Organization Code
7. Author(s) Brent A. Miller and John M. Abbott		8. Performing Organization Report No. E-7372
		10. Work Unit No. 501-24
9. Performing Organization Name and Address Lewis Research Center National Aeronautics and Space Administration Cleveland, Ohio 44135		11. Contract or Grant No.
		13. Type of Report and Period Covered Technical Memorandum
12. Sponsoring Agency Name and Address National Aeronautics and Space Administration Washington, D.C. 20546		14. Sponsoring Agency Code
15. Supplementary Notes		

16. Abstract

Low-speed wind-tunnel tests were conducted to determine the effects of free-stream velocity and incidence angle on the aerodynamic and acoustic performance of a translating centerbody choked-flow inlet. The inlet was sized to fit a 13.97 cm diameter fan with a design weight flow of 2.49 kg/sec. Performance was determined at free-stream velocities to 45 meters per second and incidence angles of 0° to 50°. The inlet was operated in both the choked and unchoked modes over a range of weight flows. Measurements were made of inlet total-pressure recovery, flow distortion, surface static pressure distribution, and fan noise suppression. In the choked mode, increasing incidence angle tended to reduce the amount of inlet noise suppression for a given amount of inlet suction. This tendency was overcome by applying sufficient inlet suction to increase the flow Mach number. At 45 meters per second free-stream velocity, at least 22 decibels of suppression were measured at 35° incidence angle with a total pressure recovery of 0.985. Increasing incidence angle generated total pressure distortions primarily by concentrating existing total pressure losses in the bottom, or windward, portion of the inlet.

17. Key Words (Suggested by Author(s)) Inlet design; Sonic inlet; Choked inlet; Acoustic suppression; Pressure recovery; Noise reduction; Wind-tunnel tests		18. Distribution Statement Unclassified - unlimited	
19. Security Classif. (of this report) Unclassified	20. Security Classif. (of this page) Unclassified	21. No. of Pages 32	22. Price* $3.00

* For sale by the National Technical Information Service, Springfield, Virginia 22151

LOW-SPEED WIND-TUNNEL INVESTIGATION OF THE AERODYNAMIC AND ACOUSTIC PERFORMANCE OF A TRANSLATING-CENTERBODY CHOKED-FLOW INLET

by Brent A. Miller and John M. Abbott

SUMMARY

Low-speed wind-tunnel tests were conducted to determine the effects of free-stream velocity and incidence angle on the aerodynamic and acoustic performance of a translating-centerbody choked-flow inlet. The inlet was sized to fit a 13.97-centimeter-diameter fan with a design weight flow of 2.49 kilograms per second. Performance was determined at free-stream velocities of 24, 32, and 45 meters per second and incidence angles of 0°, 10°, 20°, 30°, 35°, 40°, 45°, and 50°. The inlet was operated in both the choked and unchoked modes over a range of weight flows. Measurements were made of inlet total-pressure recovery, flow distortion, surface static-pressure distribution, and fan noise suppression.

In the unchoked mode, inlet total-pressure recovery remained above 0.995 for all operating conditions to a 35° incidence angle. At incidence angles above 35°, flow separation was encountered, with a consequent drop in pressure recovery and increase in fan broad band noise.

In the choked mode, increasing the incidence angle tended to reduce the amount of inlet noise suppression for a given amount of inlet suction. This may have been due to the variations in throat static pressure, and hence flow Mach number, generated by increasing the incidence angle. However, this tendency was overcome by applying sufficient inlet suction to increase the flow Mach number. At a free-stream velocity of 45 meters per second, at least 22 decibels of suppression was measured at a 35° incidence angle, with a total-pressure recovery of 0.985. Increasing the incidence angle generated total-pressure distortions primarily by concentrating existing total-pressure losses in the bottom, or windward, portion of the inlet.

INTRODUCTION

Future commercial aircraft presently under study, such as the near-sonic transport, the advanced supersonic transport, and STOL aircraft, will be required to meet stringent noise specifications. The primary source of aircraft noise is the engine, and current unsuppressed designs cannot meet the future noise goals. Experiments have shown that compressor and fan noise radiating from the engine inlet can be reduced at static conditions by choking the flow with either inlet guide vanes, contracting cowl walls, or a translating centerbody (refs. 1 to 6). Further experiments are required to determine the performance of choked-flow inlets under flight conditions.

The purpose of the present investigation was to measure the effects of free-stream velocity and incidence angle on the aerodynamic and acoustic performance of a translating-centerbody choked-flow inlet. The inlet was sized to fit a 13.97-centimeter-diameter fan. Inlet performance was determined in a wind tunnel at free-stream velocities of 24, 32, and 45 meters per second and incidence angles of 0° to 50°. Inlet total-pressure recovery, flow distortion, surface static-pressure distribution, and acoustic performance are presented for the inlet operating in both the choked and unchoked modes.

SYMBOLS

D_{max} inlet total-pressure distortion parameter, (maximum total pressure - minimum total pressure)/(average total pressure)

D_{60} inlet circumferential total-pressure distortion parameter, (average total pressure - minimum average total pressure over any 60° circumferential sector)/(average total pressure)

d_t cowl throat diameter, cm

L cowl length, cm

M average throat Mach number computed with assumed one-dimensional flow

N fan rotational speed, rpm

P_0 free-stream total pressure, N/m^2

P_1 area-averaged total pressure at rake measuring plane, N/m^2

$P_{1,l}$ local total pressure at rake measuring plane, N/m^2

p_1 average tip static pressure at rake measuring plane, N/m^2

R_H flow-passage hub radius at rake measuring plane, cm

R_T flow-passage tip radius at rake measuring plane, cm

V_0 free-stream velocity, m/sec

W distance from rake measuring plane to fan rotor, cm

X axial distance from cowl highlight, cm

α incidence angle (angle between free-stream velocity and inlet centerline), deg

ΔdB reduction in 1/3-octave band sound pressure level, dB

θ fan inlet corrected temperature, (fan inlet temperature in K)/(288.2 K)

ψ inlet circumferential position, deg

APPARATUS AND PROCEDURE

Figure 1 shows the general layout of the test installation in the Lewis Research Center's 9- by 15-foot V/STOL Wind Tunnel (ref. 7). The model was mounted in the test section on a rotating turntable for testing at various incidence angles. Microphones were mounted upstream of the test section in the tunnel settling chamber to measure inlet noise. The test model consisted of a test inlet, an adapter section, a fan, exhaust ducting, and an exhaust noise muffler. The single-stage, 13.97-centimeter-diameter, tip turbine driven fan was used both as a suction source and as a noise generator. The fan has 16 rotor blades, which results in a blade passing frequency of 9600 hertz at the fan design speed of 36 000 rpm. The design pressure ratio is 1.25 at a weight flow of 2.49 kilograms per second. Inlets were mounted to the fan by use of an adapter section containing the supports for the stationary centerbody as well as the total-pressure rakes used to measure inlet performance. No measurements were taken downstream of the fan.

Inlet Design

Translating-centerbody inlet in unchoked mode. - Figure 2(a) shows the translating-centerbody inlet in the unchoked mode (centerbody retracted). This configuration resembles a conventional inlet and would be the operating mode of this inlet at cruise, where inlet choking for noise suppression is not required. The design throat Mach number is 0.6 at a weight flow of 2.49 kilograms per second. The flow area is increased 8.2 percent by the diffuser, and this results in a Mach number of 0.53 at the rake measuring plane. The effective conical half angle of the diffuser is 1.57°. The design axial Mach number distribution through the inlet is given in reference 5. Details of the cowl and spinner design are also given in reference 5. The external cowl has an NACA series 1 shape and was designed to have a drag-rise Mach number of approximately 0.80. The cowl internal lip is a two-to-one ellipse. The contraction ratio (highlight area/throat area) is 1.30. The spinner is an NACA series 1 design with a length-to-diameter ratio of 1.

Translating-centerbody inlet in choked mode. - Figure 2(b) shows the translating-centerbody inlet in the choked mode (centerbody extended). The cowl throat area was reduced 15.84 percent by using a cylindrical spacer to place the spinner in the cowl throat. This increased the diffuser effective conical half angle to 5.19°. The throat area was sized so that the choked weight flow remained constant at the unchoked value of 2.49 kilograms per second. Mach 1 occurs at the cowl throat plane, while the design Mach number at the rake measuring plane remains 0.53. The diffuser area ratio, measured between the cowl throat plane and the rake measuring plane is 1.29. The design axial Mach number distribution through the inlet is given in reference 5.

Instrumentation and Data Reduction

Test instrumentation gave measurements of inlet noise levels, inlet pressure recovery, steady-state total-pressure distortion, and surface static pressures. Detailed schematics of the instrumentation are given in reference 5.

Rake measuring plane. - As shown in figure 2, eight radial total-pressure rakes were located in the adapter section at the rake measuring plane. The rakes were spaced at 45° intervals, with six area-weighted total-pressure tubes on each rake. Seven static-pressure taps were located on the outer wall of the flow passage, between the total-pressure rakes.

Inlet cowl. - The inlet cowl was instrumented to measure surface static pressures as shown in figure 2. Eleven static-pressure taps were located in a row at the $\psi = 0^{\circ}$, or windward, circumferential position. Five taps were located on the inlet lip between the highlight and throat; the remaining six were located in the diffuser. An additional five static-pressure taps, spaced at 60° intervals, were located in the cowl throat.

Noise measurements. - Noise data were taken with four microphones located in the wind-tunnel settling chamber upstream of the test section. The hard walls of the wind tunnel approximate a reverberant chamber and eliminate any directional noise variation due to changing incidence angle. The microphone outputs were recorded on magnetic tape and then processed with a 1/3-octave band analyzer. The fan exhaust was ducted out of the test section and into a noise muffler to permit an examination of only the noise being transmitted through the inlet.

Test Procedure

An initial static calibration test was conducted with a bell-mouth inlet replacing the inlet cowl. The weight flow measured by the instrumentation at the rake measuring plane was then corrected to agree with the measured bell-mouth inlet weight flow. This correction was then applied at the appropriate fan speeds in all the data runs with the inlet cowl in place.

The tests were conducted at free-stream velocities of 0, 24, 32, and 45 meters per second, and at fan corrected speeds from 30 000 to 37 200 rpm. Incidence angles of 0°, 10°, 20°, 30°, 35°, 40°, 45°, and 50° were investigated. The test procedure consisted of setting free-stream velocity and corrected fan speed, and then varying incidence angle from 0° to 50°. The fan corrected speed was then changed, and the variation of incidence angle was repeated. After taking data at each of the fan corrected speeds, the free-stream velocity was changed. The procedure was then repeated.

RESULTS AND DISCUSSION

Inlet performance is presented in two major parts. The first part shows performance obtained with the inlet operating in the unchoked mode (centerbody retracted). With this centerbody position, the inlet remains unchoked at all fan operating speeds. The second part shows the performance obtained with the inlet operating in the choked mode (centerbody extended). This centerbody position allows the inlet to operate unchoked at low fan speeds and choked at high fan speeds.

Unchoked Operating Mode

Average throat Mach number and inlet total-pressure recovery. - The relation between average throat Mach number and inlet total-pressure recovery is shown in figure 3. Average throat Mach number was determined with the weight flow computed from the total- and static-pressure measurements at the rake measuring plane. Total-pressure recovery is based on the area-averaged total pressure at the rake measuring plane. At static conditions (fig. 3(a)), total-pressure recovery varied between 0.996 and 0.998 over the throat Mach number range from 0.505 to 0.637. This high pressure recovery at static conditions is a result of the relatively thick lip obtained with a 1.3 contraction ratio. Total-pressure recovery at a free-stream velocity of 24 meters per second is shown in figure 3(b) for incidence angles of 0°, 20°, 40°, and 50°. The data show little effect of throat Mach number on recovery. However, an increase in incidence angle does produce a small reduction in recovery. At a throat Mach number of 0.56, the recovery is reduced from 0.999 to 0.997 in going from 0° to 50° incidence angle. Increasing the free-stream velocity to 32 meters per second resulted in the recoveries shown in figure 3(c). At incidence angles of 0° to 45°, recovery decreases slightly with both increasing throat Mach number and incidence angle. However, at an incidence angle of 50°, inlet separation occurred (as will be shown later) when the average throat Mach number was increased from 0.565 to 0.582. This separation caused an abrupt drop in total-pressure recovery from 0.996 to 0.974. The result of further increasing the free-stream velocity to 45 meters per second is shown in figure 3(d). The recovery remained above 0.995 at all throat Mach numbers for incidence angles up to 35°. At 40°, separation occurred at the higher throat Mach numbers. The presence of some hysteresis is indicated by the relative position of the two data points connected by the dashed line. Inlet separation occurred at incidence angles of 45° and 50° regardless of average throat Mach number.

Several data points in figure 3(d) are labeled A, B, and C. For convenience in comparing data, these same points are labeled on several figures that follow.

The data of figure 3 indicate that this inlet will give total-pressure recoveries above 0.995 over a wide range of operating conditions. However, inlet separation, with a consequent large drop in total-pressure recovery, can be induced by operating at incidence angles above 35°. Reducing both free-stream velocity and average throat Mach number improves inlet tolerance to incidence angle. The following section presents inlet total-pressure distortion measured at the operating conditions just discussed.

Total-pressure distortion. - Total-pressure distortion measured at the rake measuring plane is shown in figure 4 as a function of average throat Mach number. The two total-pressure distortion parameters, D_{max} and D_{60}, are defined in the symbol list.

Distortions measured at static conditions are shown in figure 4(a). The figure shows a random distribution of D_{max} with throat Mach number, with the maximum measured D_{max} being approximately 0.06. As would be expected for static operation of an axisymmetric inlet, there is little or no circumferential distortion, D_{60}

The total-pressure distortion measured at a free-stream velocity of 24 meters per second is shown in figure 4(b). The dispersion noted in D_{max} at static conditions is no longer present. The data show a progressive increase in D_{max} with both increasing throat Mach number and increasing incidence angle. At a given incidence angle, the average increase in D_{max} over the throat Mach number range from 0.50 to 0.56 is approximately 0.010. A larger increase in D_{max} of 0.044 was obtained at a throat Mach number of 0.56 by increasing the incidence angle from 0° to 50°. Inlet separation encountered at a free-stream velocity of 32 meters per second and an incidence angle of 50° is clearly reflected by the distortions shown in figure 4(c). Note the large increase in both D_{max} and D_{60} associated with the total-pressure-recovery drop noted in figure 3(c). At a free-stream velocity of 45 meters per second (fig. 4(d)), inlet separation is again easily identified by the large distortion increases recorded at incidence angles of

40°, 45°, and 50°. At lower angles, note the progressive increase in D_{max} with both average throat Mach number and incidence angle.

Total-pressure contours generated at the rake measuring plane are shown in figure 5 for the data points labeled A, B, and C in figures 3(d) and 4(d). Figure 5(a) shows the low distortion levels and axisymmetric flow obtained at a 0° incidence angle. Free-stream velocity is 45 meters per second. Total-pressure recovery is 0.998.

An increase in incidence angle to 35° produced the total pressure contours shown in figure 5(b). The regions of lowest recovery are located in the lower half of the inlet, near the $\psi = 0^{\circ}$ position. Although the inlet has not separated, total-pressure recovery has fallen from 0.998 to 0.995. The inlet separation that was encountered when the incidence angle was increased from 35° to 40° is reflected by the contours of figure 5(c). Note the local region of low total pressure located on the outer wall near the $\psi = 0^{\circ}$ position. This indicates the presence of large-scale flow separation at this circumferential position. The presence of this separation is also indicated by the internal cowl-surface static-pressure distributions shown in figure 6. Here, cowl-surface static pressure is plotted as a fraction of free-stream total pressure from the highlight to the rake measuring plane at the $\psi = 0^{\circ}$ position. The free-stream velocity is 45 meters per second, and the corrected fan speed is 34 700 rpm. Increasing the incidence angle from 0° to 35° produced a progressive drop in lip static pressure, which indicates the presence of high local velocities induced by the inclined flow. Static-pressure distributions in the diffuser were relatively unaffected, which indicates no diffuser separation. However, as the incidence angle was increased from 35° (data point B) to 40° (data point C), an abrupt change occurred in both lip and diffuser pressure distributions. Lip static pressure increased, while diffuser pressure dropped. This behavior is attributed to separation occurring on the inlet lip, near the highlight, and extending completely through the throat and diffuser. A more complete discussion of this can be found in reference 5, where the present data were compared with theoretically predicted static-pressure distributions.

In summary, figures 4 and 5 show a progressive effect of incidence angle, throat Mach number, and free-stream velocity on D_{max} and D_{60}. Values of D_{max} below 0.10 were obtained over a wide range of operating conditions. The most severe distortions were encountered at the highest values of the three parameters. The large-scale flow separations that were observed appeared to originate on the inlet lip. It is possible that full-sized inlets of this contraction and diffusion ratio may be somewhat more tolerant of incidence angle than the present small-scale data would indicate.

Acoustic performance. - The effect of incidence angle on inlet radiated fan noise is shown in figure 7. The free-stream velocity is 45 meters per second. Sound pressure level is plotted against 1/3-octave band center frequency. The edge of the shaded area shows the noise floor determined by operating the wind tunnel with the model installed but not running. The fan blade passing noise in the 10 000-hertz band is approximately 22 decibels above this floor.

Changing the incidence angle from 0° to 35° had little effect on noise generation. However, with the onset of inlet flow separation at an incidence angle of 40°, a large increase occurs in the broadband noise as a result of the distorted flow passing through the fan. But note that in the 10 000-hertz band containing the fan blade passing frequency, a small reduction in noise generation can be observed.

It should be noted that for this particular installation, the fan was located some distance downstream of the rake measuring plane. Had the fan been located at the rake measuring plane, the lower incidence angles may have also changed the noise-generation characteristics of the model.

Choked Operating Mode

In the discussion of the unchoked inlet, performance was presented as a function of the average throat Mach number computed from the inlet weight flow. This method of data presentation is satisfactory as long as the average Mach number does not exceed approximately 0.70. Above this value, small errors in determining inlet weight flow produce progressively larger errors in computed Mach number. Thus, the certainty to which the average Mach number can be determined from measured weight flow diminishes as Mach 1 is approached. For this reason, average Mach number was not used as a correlating parameter for presenting data with the inlet in the choked operating mode. Instead, data are presented as a function of the ratio of the average static pressure measured at the rake measuring plane to the free-stream total pressure. This pressure ratio indicates the degree of suction applied to the inlet and was found to be useful for presenting both aerodynamic and acoustic performance. Average throat Mach number computed from the inlet weight flow is presented, however, and serves to indicate the general level of the throat velocity.

Average throat Mach number and inlet total-pressure recovery. - Average throat Mach number and inlet total-pressure recovery are shown in figure 8 as a function of rake-plane pressure ratio. Figure 8(a) shows static performance. The effect of increasing inlet suction can be seen by moving toward the left side of the figure to lower values of rake-plane static pressure. Movement in this direction initially increases the average throat Mach number, with a consequent reduction in total-pressure recovery. When the rake-plane static pressure is decreased sufficiently, the critical condition is reached, and an average Mach number of 1.0 exists at the throat. Further reductions in rake-plane static pressure result in supercritical operation, with no increase in average throat Mach number. However, the pressure recovery continues to drop. Data points D and E are labeled in the figure and are indicated in several following figures for convenience in comparing data. Data point D, with an average throat Mach number of 0.865

and a total pressure recovery of 0.984, will be shown in a later figure to provide the maximum measurable acoustic suppression at the fan blade passing frequency. The solid lines are least-squares curve fits to the data.

Data obtained at a free-stream velocity of 24 meters per second are shown in figure 8(b). Incidence angles of 0°, 20°, 40°, and 50° are indicated. The curve fit to the static data is shown by the dashed line and indicates little or no measurable effect of free-stream velocity or incidence angle on total-pressure recovery. The effect of increasing the free-stream velocity to 32 meters per second is shown in figure 8(c). Note that the data closely match the static-data curve-fit line. Again, little effect of incidence angle on total-pressure recovery can be detected over the range of 0° to 50°. The total-pressure recoveries below 0.97 were caused by supercritical operation, not by operating inclined to the free-stream velocity. The effect of further increasing the free-stream velocity to 45 meters per second is indicated by figure 8(d). Some systematic effect of incidence angle on total-pressure recovery can now be detected. For example, at a rake-plane pressure ratio of approximately 0.83, increasing the incidence angle from 0° to 50° produced a 0.005 drop in total pressure recovery. However, the data remain reasonably close to the static-data curve-fit line. Several data points are labeled in the figure for convenience in comparing data in later figures. The proximity of point H to the dashed line indicates that the low value of total-pressure recovery measured can be attributed to supercritical inlet operation, not to the 50° incidence angle. However, the total-pressure recovery of point I is considerably below the dashed line, which indicates the presence of losses induced by effects other than supercritical operation. An examination of the axial variation of inlet-surface static pressure at this point indicated a profile similar to that shown by data point C in figure 6. This similarity suggests that the low total-pressure recovery (P_1/P_0 = 0.951) of point I was caused by separation occurring near the highlight because of the 50° incidence angle. This point is unique in that it is the only data point obtained with the inlet in the choked mode that indicates incidence-angle-induced lip flow separation.

Summarizing figure 8, the data indicate little effect of incidence angle on total-pressure recovery at free-stream velocities of 24 and 32 meters per second. At these conditions, as well as statically, total-pressure recovery is primarily a function of the suction applied to the inlet. However, at a free-stream velocity of 45 meters per second, some effect of incidence angle can be detected. One data point in particular shows a low total-pressure recovery that is attributed to incidence-angle effects.

Total- and static-pressure distortions. - The total-pressure distortion measured at the inlet operating conditions discussed in the previous section is shown in figure 9. Figure 9(a) indicates a general increase in the total pressure distortion measured statically, with decreasing rake-plane pressure ratio. This trend reflects the losses generated by increasing the average throat Mach number. At data point D, the distortion parameters

D_{max} and D_{60} are 0.114 and 0.0046, respectively. At data point E, where the inlet is operating supercritically, D_{max} has increased to 0.222. Note the increase in D_{60} to 0.014. As mentioned previously, the distortion parameter D_{60} is a measure of the circumferential variation of distortion and would be zero for axisymmetric flow, regardless of the value of D_{max}.

The effect of increasing incidence angle on total-pressure distortion at a free-stream velocity of 24 meters per second is shown in figure 9(b). The data clearly indicate an increase in D_{max} with both increasing incidence angle and increasing inlet suction.

Increasing the free-stream velocity to 32 meters per second produced the total-pressure distortion shown in figure 9(c). Again, note the progressive increase in D_{max} with incidence angle and applied suction. The effect of further increasing the free-stream velocity to 45 meters per second is indicated in figure 9(d). At a rake-plane pressure ratio of approximately 0.805, corresponding to an average throat Mach number in excess of 0.85 (see fig. 8(d)), data points F and G show D_{max} increasing from 0.075 to 0.146 in going from an incidence angle of 0° to 35°. The corresponding increase in D_{60} is from 0.0012 to 0.012.

The larger distortions shown to the left of the critical operation line are attributed to the combined effects of supercritical operation and high incidence angles. As shown in figure 8, supercritical operation generates total-pressure losses that are nearly independent of incidence angle. However, at high incidence angles, the total-pressure losses generated by supercritical operation were concentrated at one circumferential position. This resulted in large values of D_{max} and D_{60}. The high values of D_{60} recorded at points H and I indicate the presence of large circumferential distortions. This migration of existing losses to a preferred location can be seen on the total-pressure contour plots that follow.

Figure 10 shows the total-pressure contours generated at the rake measuring plane for data points D and E. Both figures show that static operation of the choked inlet produced primarily a tip radial distortion pattern. The effect of supercritical operation can be seen by comparing figures 10(a) and (b).

Total-pressure contours generated at a free-stream velocity of 45 meters per second are shown in figure 11 for data points F, G, and H. The contours for data point F (fig. 11(a)) indicate the presence of axisymmetric flow. This is the expected result at a 0° incidence angle. The contours for data point G (fig. 11(b)) reflect the effect of increasing the incidence angle to 35°. Note that the regions of lowest total pressure have migrated to the lower half of the inlet. The total-pressure recovery has decreased slightly, from 0.988 to 0.985, as a result of the increasing incidence angle. However, no indications can be seen of large-scale flow separation.

The total-pressure contours measured at 50° incidence angle (data point H) are shown in figure 11(c). Note the similarity between this figure and figure 5(c), which shows the separation encountered with the inlet operating in the unchoked mode (data point C). Although the two contour maps are similar, subsequent examination and comparison of the respective diffuser static-pressure distributions will reveal a marked difference in the type of separation producing the two contours.

Figure 12 shows the internal cowl static pressure distributions measured statically at data points D and E. Note that supercritical operation (point E) produces diffuser separation downstream of the cowl throat. This separation may be induced by a shock - boundary-layer interaction phenomenon. The separation was shown to be approximately axisymmetric in the contour plot of figure 10(b).

The circumferential variation of throat static pressure with incidence angle is shown in figure 13(a) for average throat Mach numbers ranging from 0.78 to 0.83. The corresponding axial distributions of cowl static pressure are given in figure 13(b). The free-stream velocity is 45 meters per second. Figure 13(a) shows a large effect of incidence angle on cowl throat static pressure. As would be expected, increasing the incidence angle reduced the surface static pressure on the lower half of the inlet throat while increasing it in the upper half. The implications of this static-pressure nonsymmetry, or distortion, are clear when it is recognized that the hoped for acoustic suppression is a function of the local Mach number. Thus, noise propagation paths may be formed as a consequence of the lower surface Mach numbers generated by operating inclined to the free-stream velocity. In figure 13(b), the static-pressure taps spaced axially from highlight to throat clearly show this incidence-angle effect. However, static-pressure measurements downstream of the throat in the diffuser show little change with incidence angle. This indicates little or no diffuser separation at these average throat Mach numbers.

The effect of operating at higher average throat Mach numbers (0.86 and above) is shown by figures 13(c) and (d). Note that increasing the average throat Mach number reduced the circumferential variation in throat static pressure caused by increasing the incidence angle. This can be seen by comparing figures 13(a) and (c). However, the axial static-pressure distributions of figure 13(d) indicate the presence of both throat and diffuser separations at higher throat Mach numbers. At incidence angles of 0° and 10°, a small flat region can be seen in the static-pressure distribution in the throat. This is attributed to the formation of a local separation bubble, with flow reattachment occurring immediately downstream. This reattachment occurred with little loss in inlet static pressure. As the incidence angle was increased to 20°, 30°, and 35°, the separated region grew, and reattachment occurred at X/L values between 0.30 and 0.43. Again, little loss in static pressure was measured. At incidence angles of 40° and 45°, separation again occurred downstream of the throat, and reattachment occurred at an X/L value of approximately 0.43. However, a substantial loss in static pressure was measured downstream of the reattachment point. At an incidence angle of 50° (data point H), diffuser separation occurred downstream of the throat at an X/L value of approximately 0.40 and persisted through the diffuser.

The total-pressure contour map generated at point H (fig. 11(c)) was shown to be similar to that obtained when inlet separation was encountered with the inlet operating in the unchoked mode at high incidence angles (fig. 5(c)). However, a comparison of the respective inlet axial static-pressure distributions, shown in figure 13(d) and figure 6, indicates a marked difference in the nature of the flow separation producing the similar contour plots. Figure 6 shows that the separation due to high incidence angle occurred near the inlet highlight. Figure 13(d) shows that the separation measured at data point H occurred well within the diffuser. This type of flow separation is similar to that obtained by supercritical inlet operation. This can be seen by comparing it with the axial static-pressure distribution shown by data point E in figure 12. Both points have a similarly shaped axial static-pressure distribution even though data point E was obtained at static conditions. Comparison of total-pressure contour maps for data points E (fig. 10(b)) and H (fig. 11(c)) indicates that operation at the high incidence angle has served to concentrate existing total-pressure losses at some preferred circumferential location, with a consequent increase in distortion.

In summary, increasing the incidence angle was shown to generate total-pressure distortions by concentrating existing total-pressure losses at one circumferential position. Only one data point (point I) could be identified that indicated incidence-angle-induced flow separation with the consequent distortion increase. Circumferential distortions in throat static pressure induced by incidence angle effects were measured that could adversely effect the acoustic suppression properties of the inlet.

Acoustic performance. - The effect of incidence angle on inlet radiated fan noise is shown in figure 14. Free-stream velocity is 45 meters per second. Sound pressure level is plotted against 1/3-octave band center frequency. The edge of the shaded area across the bottom of the figure shows the noise floor determined by operating the wind tunnel with the model installed but not running. The shaded area across the top of the figure shows the fan noise measured with the inlet operating in the unchoked mode. This band is a repeat of the data shown in figure 7. The data points show the noise measured with the fan operating and the inlet in the choked mode. The detectable acoustic suppression obtained with the choked inlet is defined as the difference between any data point and the appropriate point within the cross-hatched band. This acoustic suppression is indicated at the fan blade passing frequency by ΔdB. At all frequency bands, the data points closely follow the tunnel alone noise generation, suggesting that the detectable acoustic suppression is limited by the wind tunnel alone noise floor.

The sound-pressure-level reduction in the 1/3-octave band containing the fan blade passing frequency is shown in figure 15. The reduction in blade passing frequency sound pressure level was obtained by subtracting the value measured with the inlet in the choked mode from the value obtained with the inlet in the unchoked mode. This subtraction was done with the fan at approximately the same corrected speed for both modes of operation.

The suppression measured statically is shown in figure 15(a). A limit in the measurable suppression, determined by the difference in unsuppressed fan noise and the test-installation noise floor, is shown by the cross-hatched band. The test-installation noise floor was defined by the noise level measured with the model installed but not operating. Note the rapid increase in suppression with reduced rake-plane static pressure. At point D, where the measured suppression of 32 decibels just appears to intercept the noise-floor limit, the total-pressure recovery is 0.984. The average throat Mach number was computed to be 0.865. Points to the left of this show suppression measurements limited by the test-installation noise floor.

The suppression measured at a free-stream velocity of 32 meters per second is shown in figure 15(b) for incidence angles from 0° to 50°. The dashed line is a repeat of the suppression measured at zero free-stream velocity. Note that the bulk of the data points lie above this line, which indicates an improvement in suppression with free-stream velocity. The limit in the measurable suppression has been reduced because of the increased test-installation noise floor with the wind tunnel operating. Figure 15(c) shows the suppression measured at a free-stream velocity of 45 meters per second. Again, the dashed line represents the data for zero free-stream velocity. Note that data points F, G, and H are indicated in this figure. At a 0° incidence angle (data point F), the maximum detectable suppression of 22 decibels was measured in blade passing fan noise. Pressure recovery for point F is 0.988. At data point G, where the incidence angle is 35°, the maximum detectable suppression of 22 decibels was also measured. Total-pressure recovery at this point is 0.985. The three data points on the left side of this figure, including point H, show that the maximum detectable suppression was also obtained at incidence angles of 40°, 45°, and 50°. However, because of inadvertent supercritical operation, the total-pressure recovery at these points is below 0.950. Recall that figure 13(d) indicated the presence of diffuser separation at data point H. Figure 15(c) shows that this flow separation, which occurred downstream of the throat region, did not affect the detectable acoustic suppression.

Figure 15(c) does not show data points having high acoustic suppression and high total-pressure recovery at incidence angles of 40°, 45°, and 50°. However, this may be because of data point spacing and not because of limits imposed by incidence-angle effects.

Figures 15(b) and (c) indicate a trend toward lower noise suppression at a given value of inlet suction as incidence angle is increased. This may be because of the lower throat surface Mach numbers generated by operating inclined to the free-stream velocity, as pointed out in the discussion of figure 13. This effect of incidence angle on the acoustic performance of the inlet can be overcome by increasing the amount of suction applied to the inlet as incidence angle is increased. However, increasing the amount of inlet suction results in lower total-pressure recovery and higher total-pressure distortion, as previously shown in figures 8 and 9. Thus, some penalty in aerodynamic performance may result if a given noise reduction is to be maintained as incidence angle is increased.

SUMMARY OF RESULTS

The aerodynamic and acoustic performance of a translating-centerbody choked-flow inlet was determined in a low-speed wind tunnel. Effects of free-stream velocity and incidence angle were investigated with the following results:

1. In the unchoked mode, inlet total-pressure recoveries above 0.995, and total pressure distortions (D_{max}) below 0.10, were obtained for all operating conditions at incidence angles to 35°. However, inlet flow separation, with a consequent drop in total-pressure recovery and increase in distortion, was encountered at incidence angles above 35°.

2. In the unchoked mode, changes in incidence angle below that required to cause inlet flow separation had little effect on noise generation. However, a large increase in broadband noise was noted when the incidence angle was increased sufficiently to cause inlet flow separation.

3. In the choked mode, at a free-stream velocity of 45 meters per second, some effect of incidence angle on total pressure recovery was detected. For the majority of cases, however, pressure recovery was found to be a function only of the suction applied to the inlet. Increasing the incidence angle generated total-pressure distortions primarily by concentrating existing total-pressure losses in the bottom, or windward, portion of the inlet.

4. In the choked mode, at zero free-stream velocity, a 32-decibel reduction in fan blade passing noise was obtained by operating at an average throat Mach number of 0.865. Total-pressure recovery was 0.984, with total-pressure distortions, D_{max} and D_{60}, of 0.114 and 0.0046, respectively.

5. In the choked mode, increasing the incidence angle tended to reduce the amount of inlet noise suppression for a given amount of inlet suction. This may have been because of the variations in throat static pressure, and hence flow Mach number, generated by increasing the incidence angle. However, this tendency toward reduced suppression with increasing incidence angle was overcome by applying sufficient inlet suction to increase the flow Mach number. At a free-stream velocity of 45 meters per second, at least 22 decibels of suppression was measured in fan blade passing noise at a 35° incidence angle. Average throat Mach number was 0.876, with a total-pressure recovery of 0.985. Total-pressure distortions, D_{max} and D_{60}, were 0.146 and 0.012, respectively. At the same

free-stream velocity and a 0^{0} incidence angle, the same 22-decibel noise suppression was measured for an average throat Mach number of 0.867 and a total-pressure recovery of 0.988. Total-pressure distortions D_{max} and D_{60} at this point were 0.075 and 0.0012, respectively.

Lewis Research Center,
National Aeronautics and Space Administration,
Cleveland, Ohio, April 3, 1973,
501-24.

REFERENCES

1. Chestnutt, David: Noise Reduction by Means of Inlet-Guide-Vane Choking in an Axial-Flow Compressor. NASA TN D-4682, 1968.
2. Handcock, J. P.; and Hinson, B. L.: Inlet Development for the L-500. Paper 69-448, AIAA, June 1969.
3. Anon.: Study and Development of Turbofan Nacelle Modifications to Minimize Fan-Compressor Noise Radiation. Volume V - Sonic Inlet Development. NASA CR-1715, 1971.
4. Lumsdaine, Edward: Development of a Sonic Inlet for Jet Aircraft. Inter-Noise 1972 Proceedings, Washington, D.C., Oct. 4-6, 1972, pp. 501-506.
5. Miller, Brent A.; and Abbott, John M.: Aerodynamic and Acoustic Performance of Two Choked-Flow Inlets Under Static Conditions. NASA TM X-2629, 1972.
6. Klujber, F.: Results of an Experimental Program for the Development of Sonic Inlets for Turbofan Engines. Paper 73-222, AIAA, Jan. 1973.
7. Yuska, Joseph A.; Diedrich, James H.; and Clough, Nestor: Lewis 9- by 15-Foot V/STOL Wind Tunnel. NASA TM X-2305, 1971.
8. Albers, James A.: Theoretical and Experimental Internal Flow Characteristics of a 13.97-Centimeter-Diameter Inlet at STOL Takeoff and Approach Conditions. NASA TN D-7185, 1973.

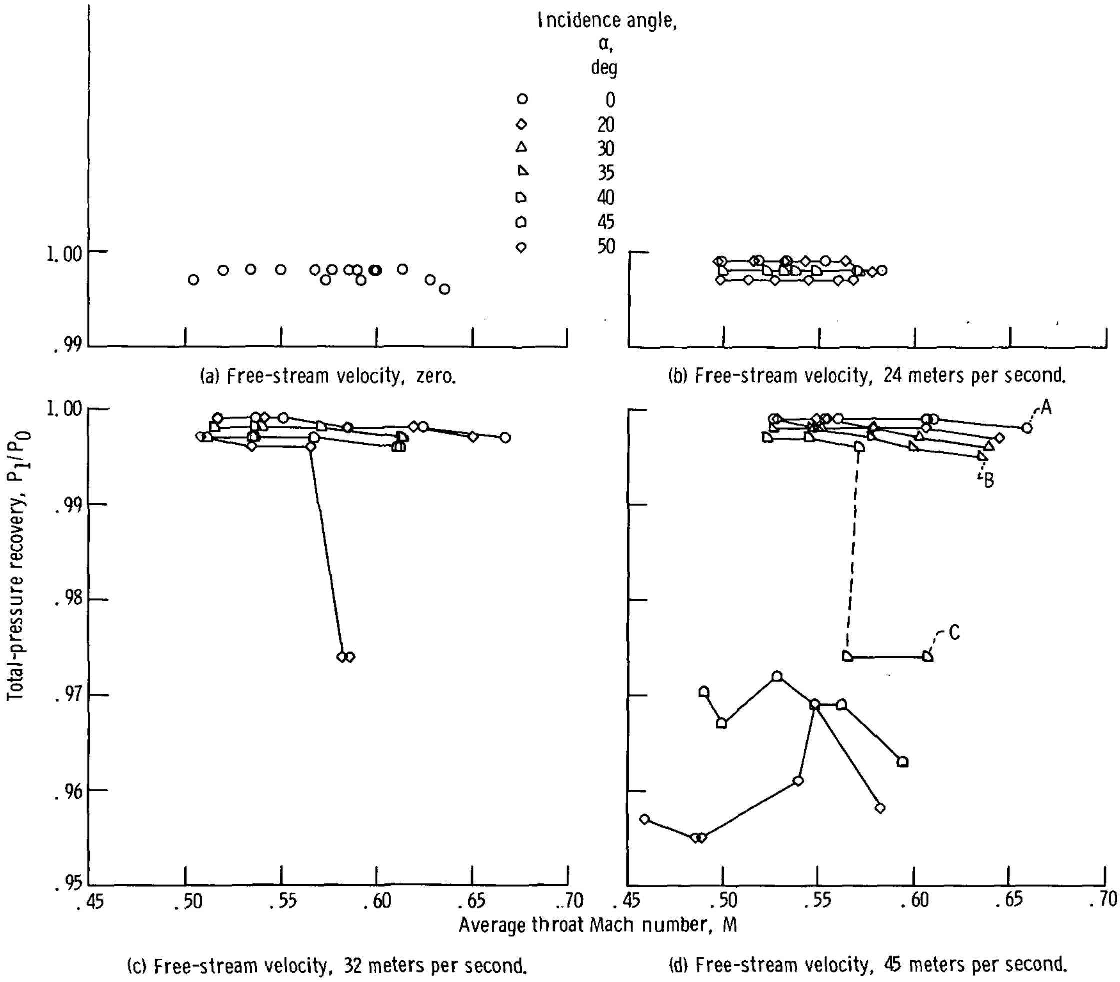

Figure 3. - Pressure recovery of translating-centerbody inlet in unchoked mode (centerbody retracted). Corrected fan speed, $N/\sqrt{\theta}$, 30 000 to 35 000 rpm.

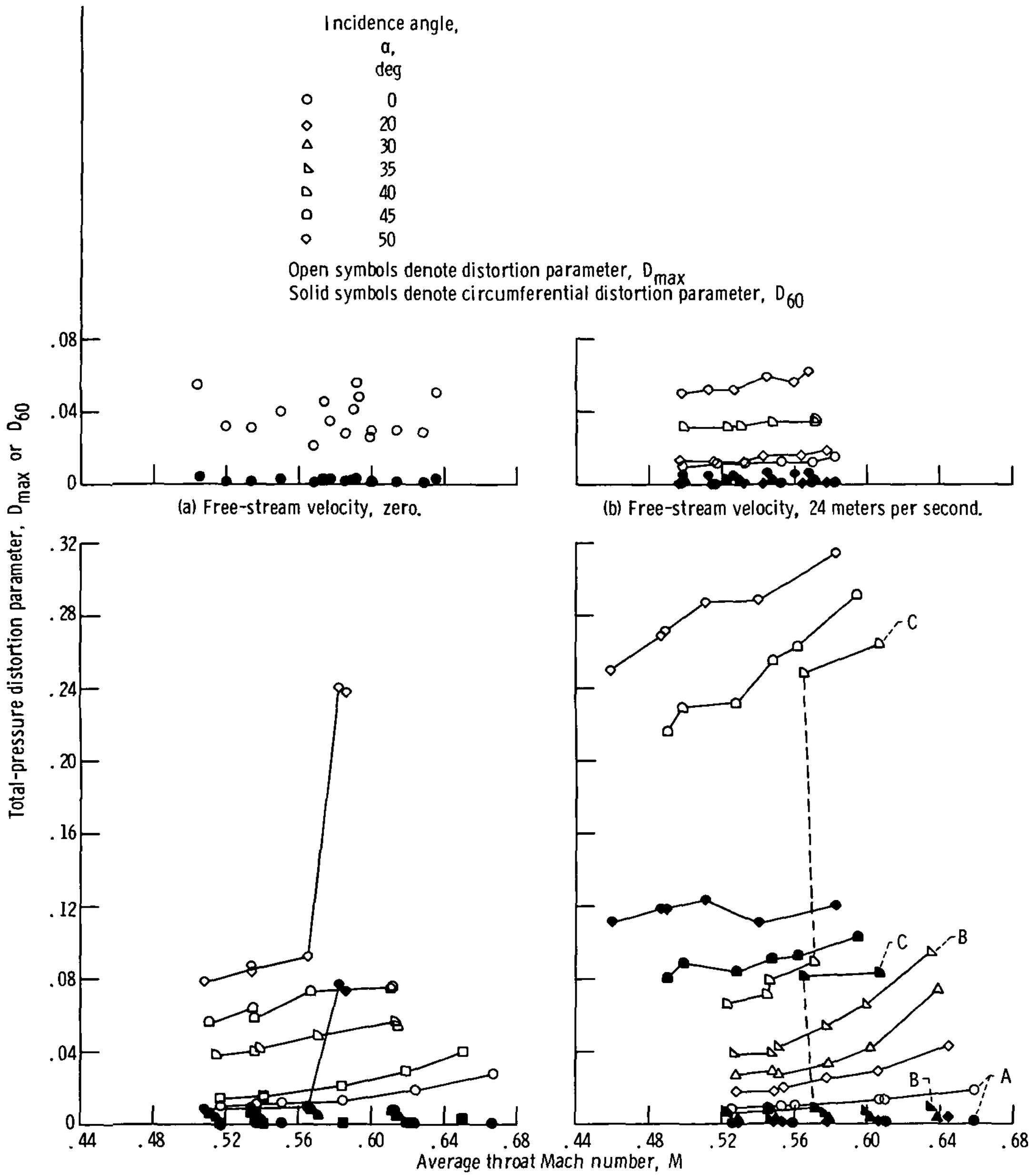

(a) Free-stream velocity, zero.

(b) Free-stream velocity, 24 meters per second.

(c) Free-stream velocity, 32 meters per second.

(d) Free-stream velocity, 45 meters per second.

Figure 4. - Total-pressure distortion generated by translating-centerbody inlet in unchoked mode (centerbody retracted). Corrected fan speed, $N/\sqrt{\theta}$, 30 000 to 35 000 rpm.

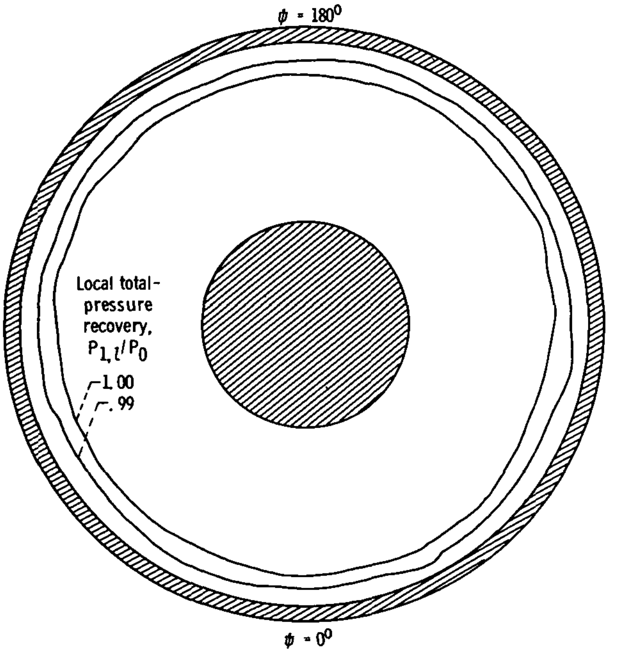

(a) Incidence angle, zero; average throat Mach number, 0.659; total-pressure recovery, 0.998; total-pressure distortion parameter, D_{max}, 0.019; circumferential total-pressure distortion parameter, D_{60}, 0.0013. (Data points A in figs. 3(d) and 4(d).)

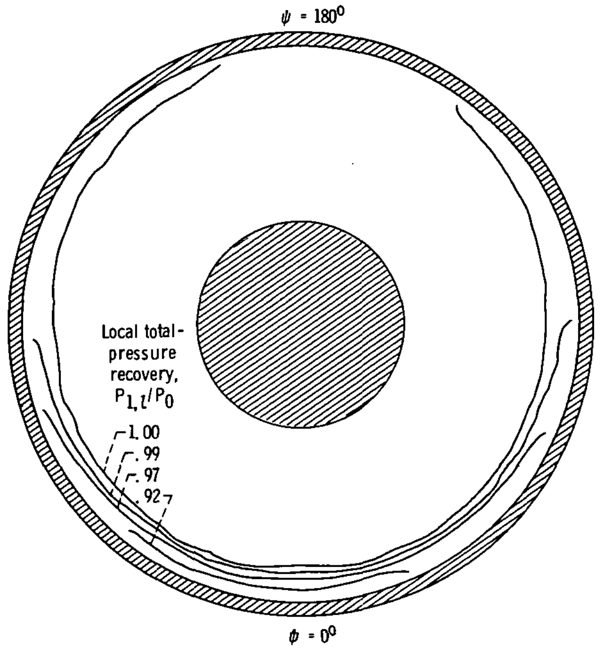

(b) Incidence angle, 35°; average throat Mach number, 0.635; total-pressure recovery, 0.995; total-pressure distortion parameter, D_{max}, 0.094; circumferential total-pressure distortion parameter, D_{60}, 0.0096. (Data points B in figs. 3(d) and 4(d).)

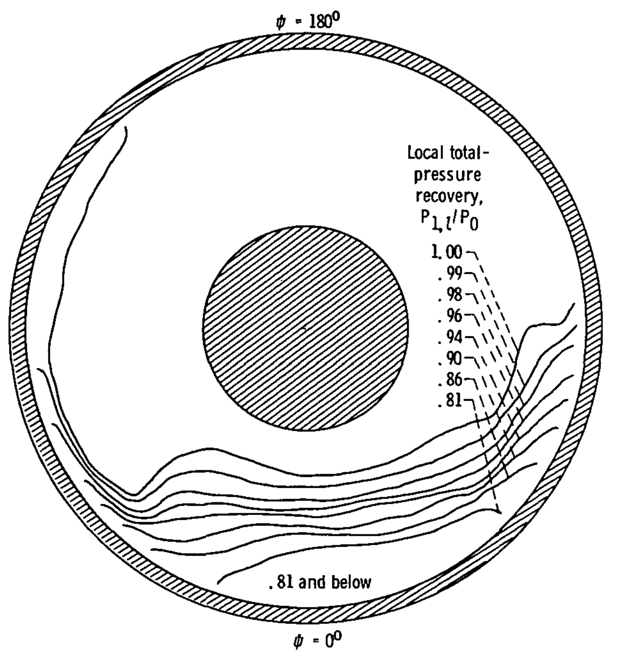

(c) Incidence angle, 40°; average throat Mach number, 0.607; total-pressure recovery, 0.974; total-pressure distortion parameter, D_{max}, 0.264; circumferential total-pressure distortion parameter, D_{60}, 0.083. (Data points C in figs. 3(d) and 4(d).)

Figure 5. - Total-pressure contours at rake measuring plane for translating-centerbody inlet in unchoked operating mode (centerbody retracted). Free-stream velocity, 45 meters per second; corrected fan speed, $N/\sqrt{\theta}$, 34 700 rpm.

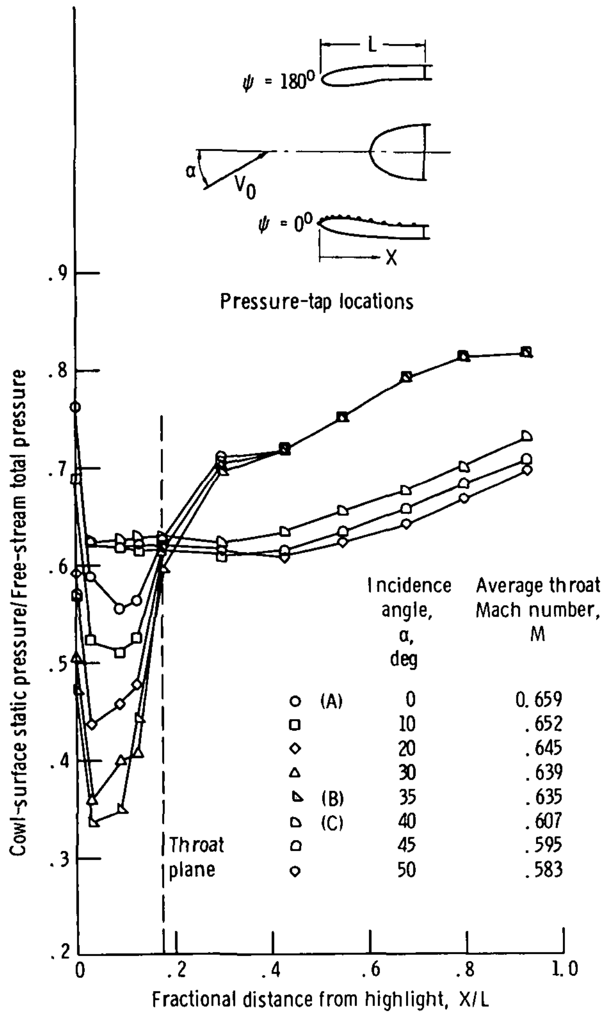

Figure 6. - Effect of incidence angle on axial variation of surface pressure ratio for a translating-centerbody inlet in unchoked operating mode (centerbody retracted). Free-stream velocity, 45 meters per second; corrected fan speed, $N/\sqrt{\theta}$, 34 700 rpm.

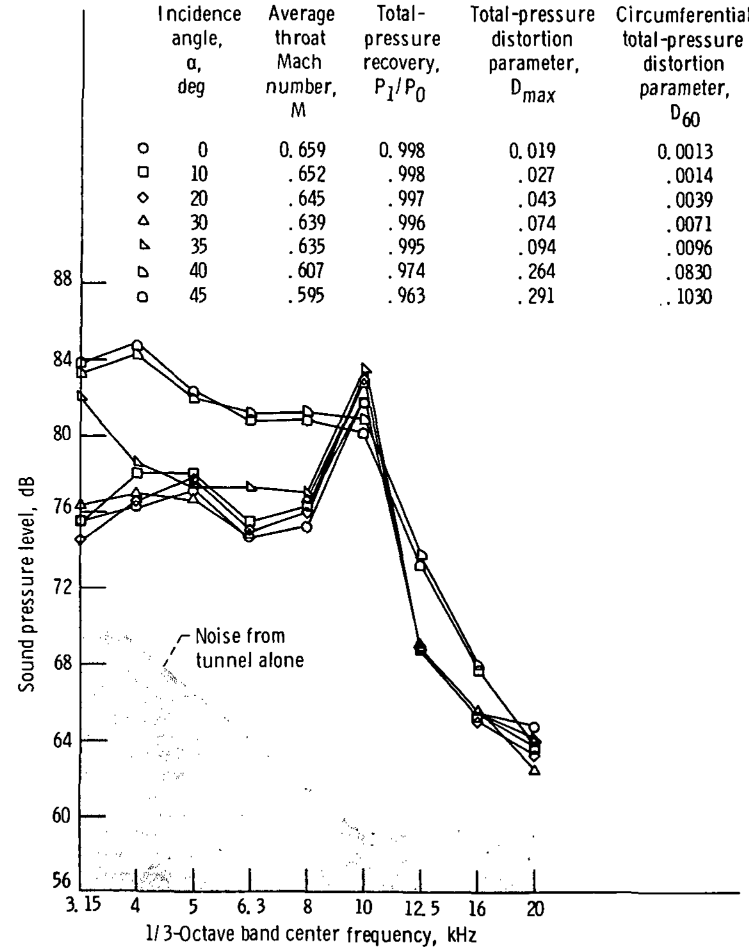

Figure 7. - Effect of incidence angle on noise of a translating-centerbody inlet in unchoked mode (centerbody retracted). Free-stream velocity, 45 meters per second; corrected fan speed, $N/\sqrt{\theta}$, 34 700 rpm.

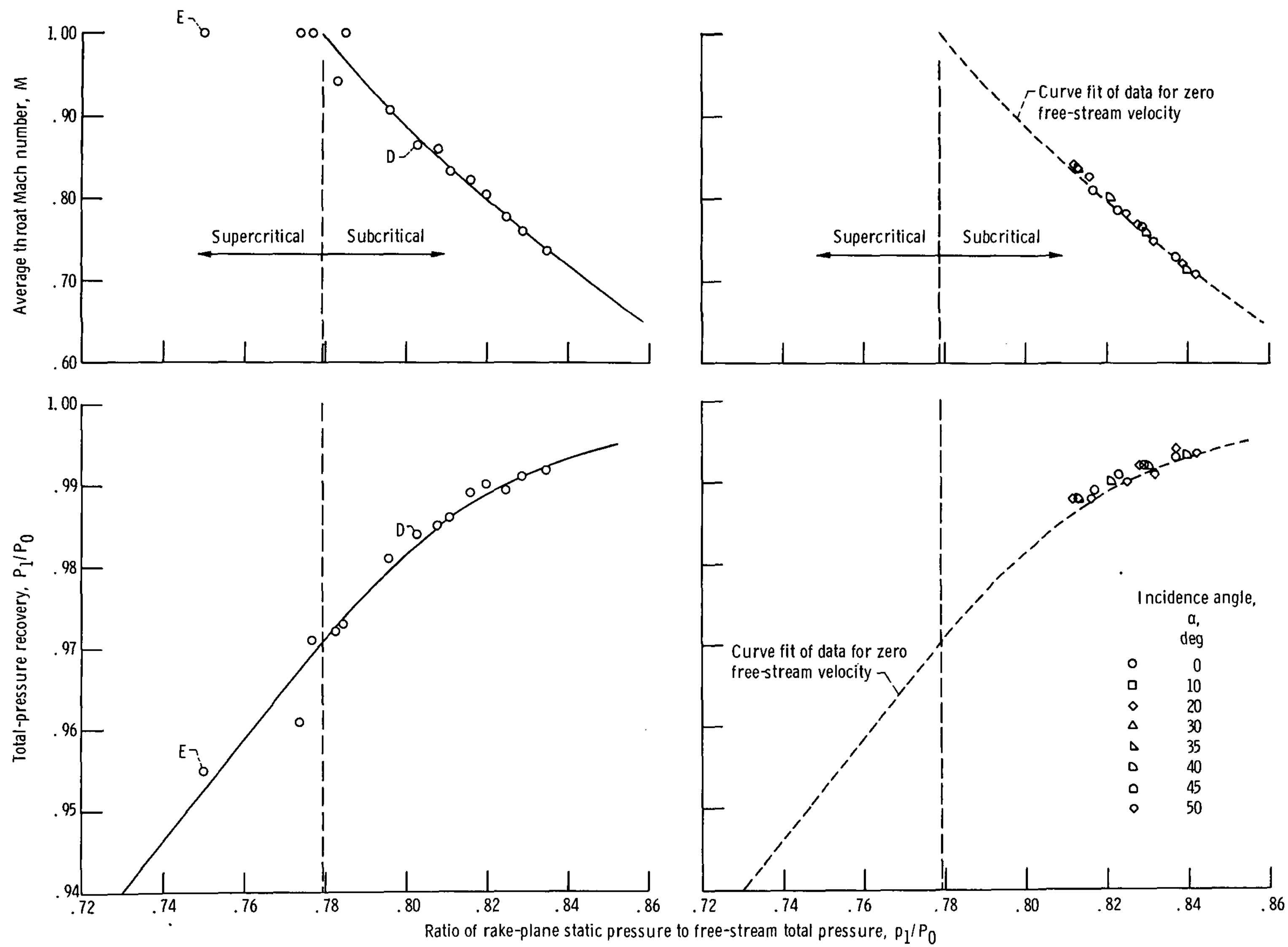

(a) Free-stream velocity, zero.

(b) Free-stream velocity, 24 meters per second.

Figure 8. - Average throat Mach number and inlet pressure recovery of translating-centerbody inlet in choked operating mode (centerbody extended). Corrected fan speed, $N/\sqrt{\theta}$, 30 000 to 37 200 rpm.

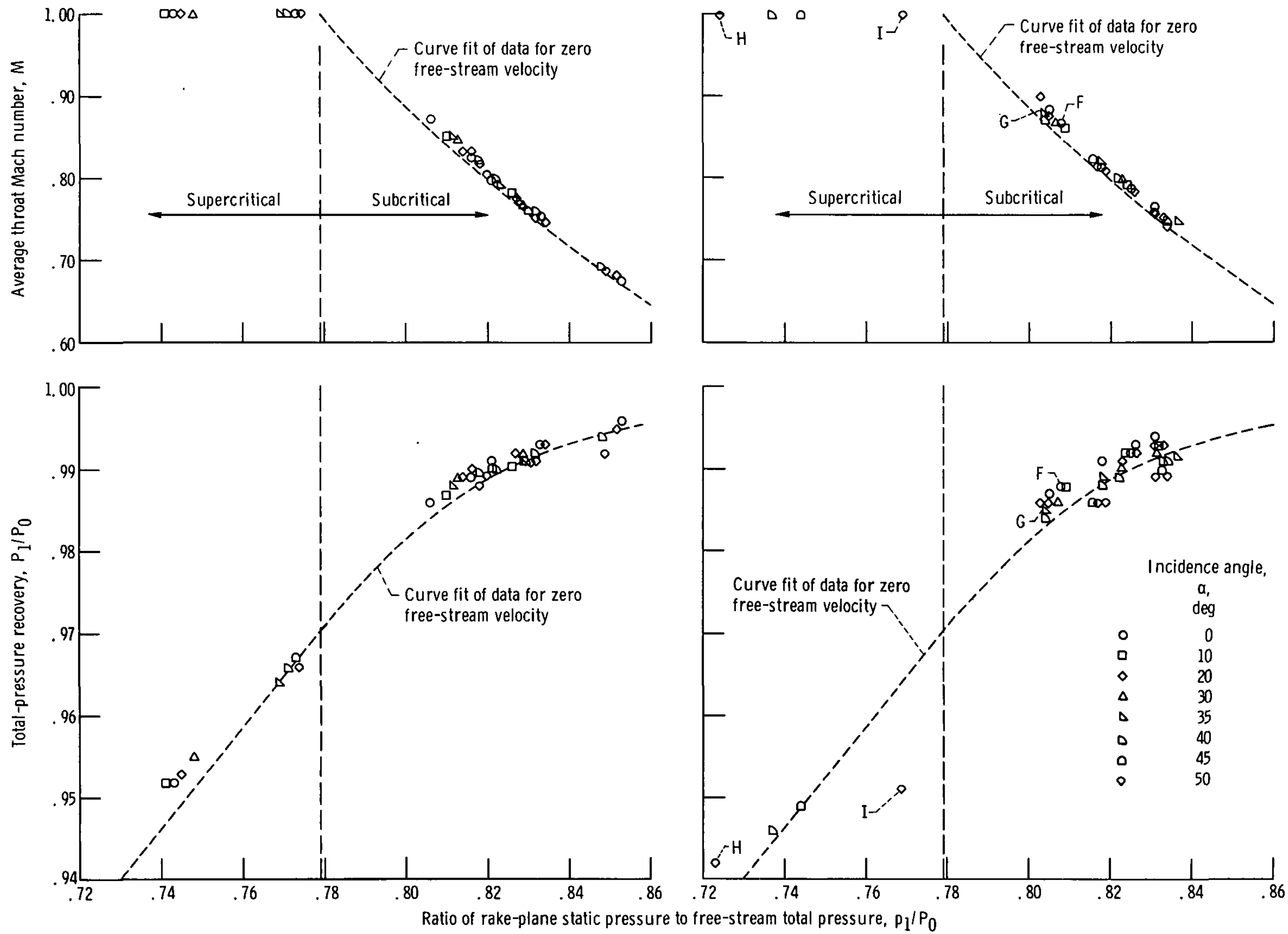

(c) Free-stream velocity, 32 meters per second.

(d) Free-stream velocity, 45 meters per second.

Figure 8. - Concluded.

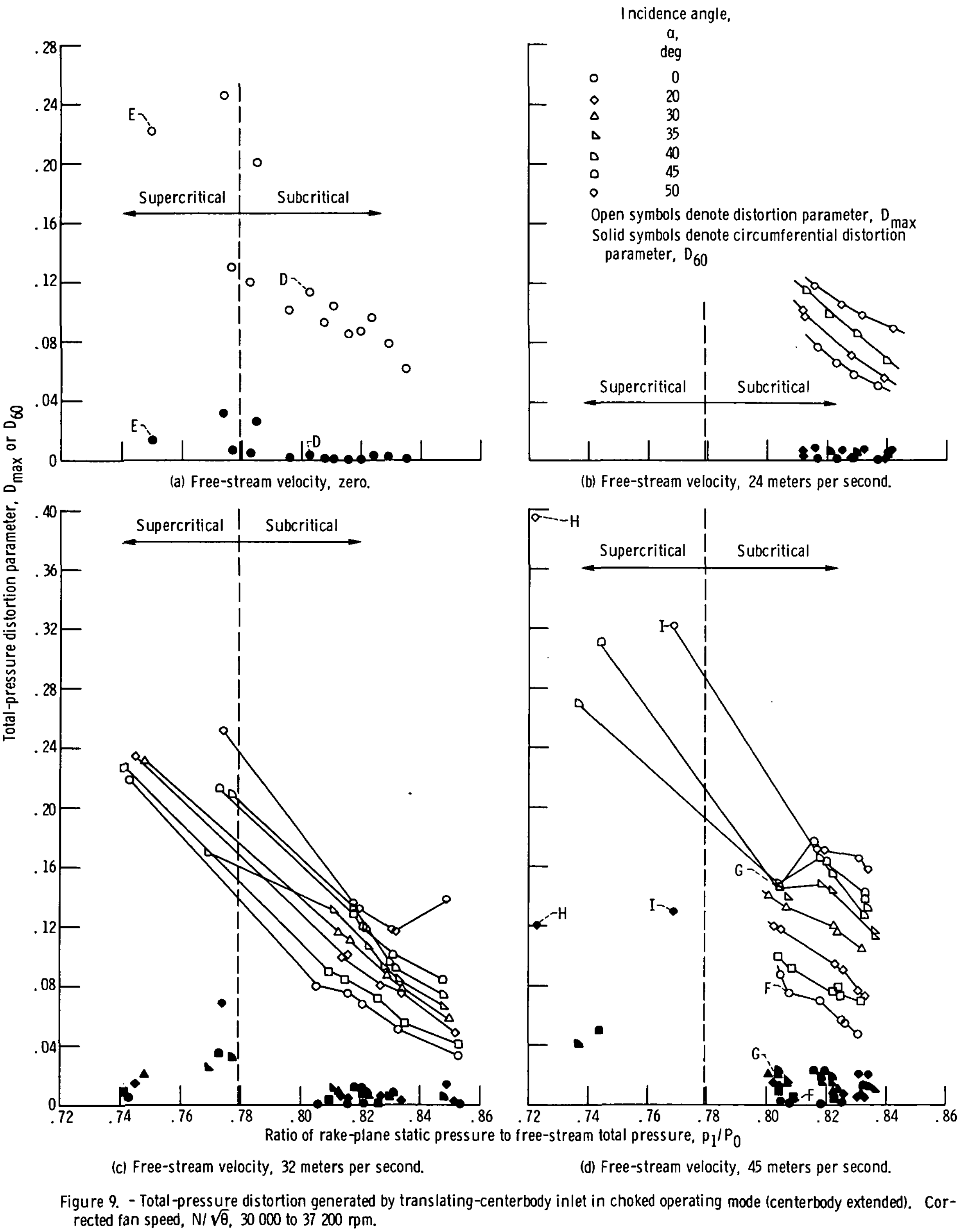

Figure 9. - Total-pressure distortion generated by translating-centerbody inlet in choked operating mode (centerbody extended). Corrected fan speed, $N/\sqrt{\theta}$, 30 000 to 37 200 rpm.

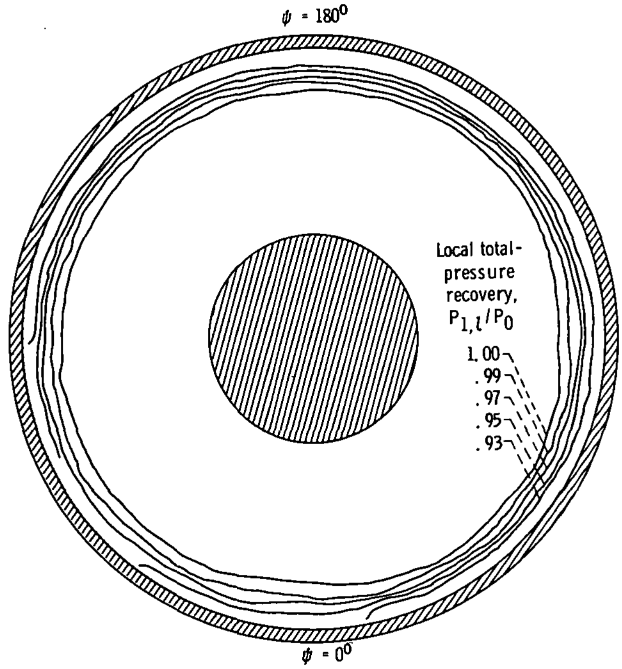

(a) Average throat Mach number, 0.865; total-pressure recovery, 0.984; total-pressure distortion parameter, D_{max}, 0.114; circumferential total-pressure distortion parameter, D_{60}, 0.0046; corrected fan speed, $N/\sqrt{\theta}$, 32 750 rpm. (Data points D in figs. 8(a) and 9(a).)

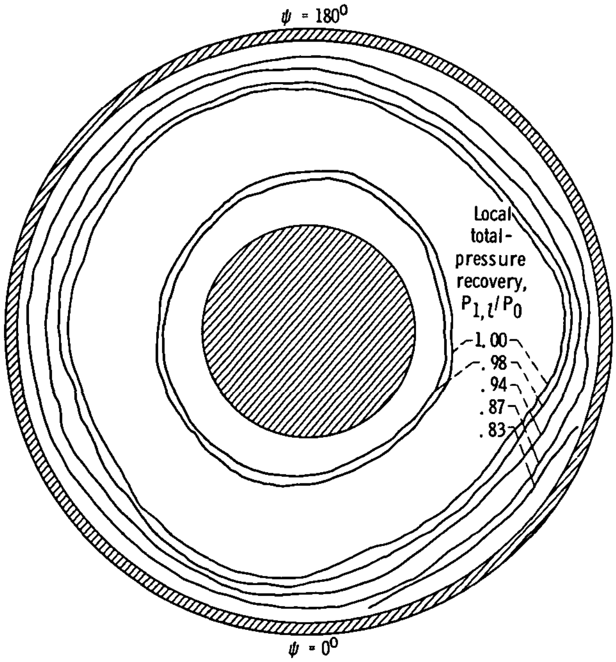

(b) Average throat Mach number, 1.0; total-pressure recovery, 0.955; total-pressure distortion parameter, D_{max}, 0.222; circumferential total-pressure distortion parameter, D_{60}, 0.014; corrected fan speed, $N/\sqrt{\theta}$, 37 200 rpm. (Data points E in figs. 8(a) and 9(a).)

Figure 10. - Total-pressure contours at rake measuring plane for translating-centerbody inlet in choked operating mode (centerbody extended). Free-stream velocity, zero.

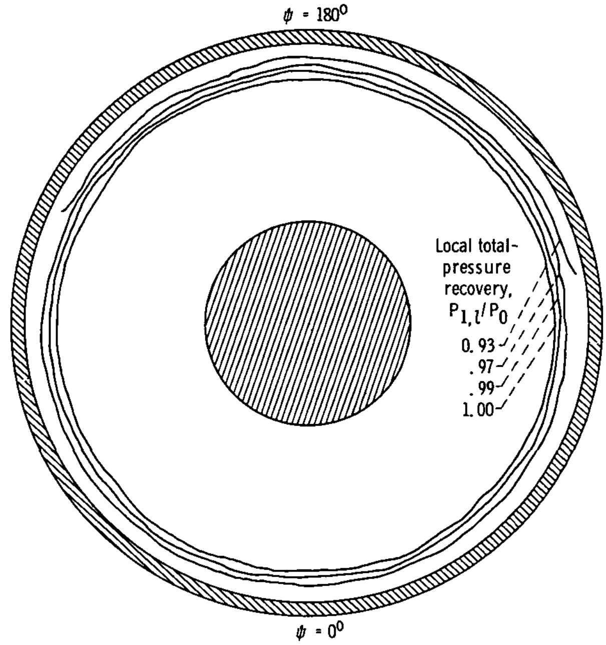

(a) Incidence angle, zero; average throat Mach number, 0.867; total-pressure recovery, 0.988; total-pressure distortion parameter, D_{max}, 0.075; circumferential total-pressure distortion parameter, D_{60}, 0.0012. (Data points F in figs. 8(d) and 9(d).)

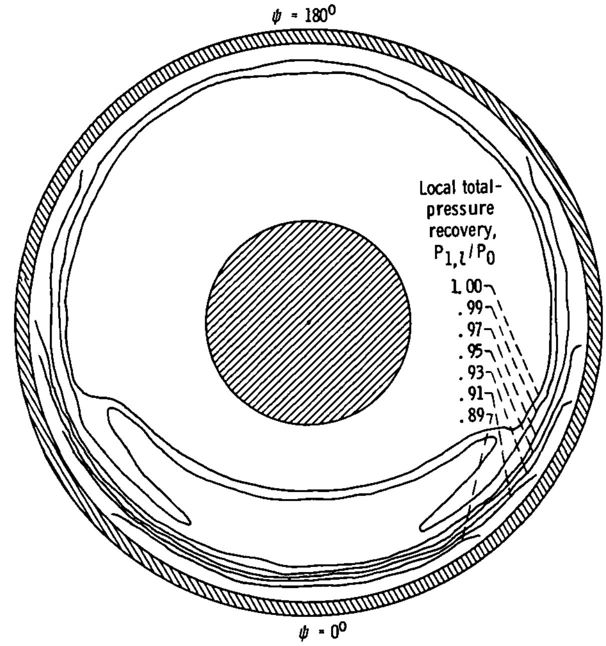

(b) Incidence angle, 35°; average throat Mach number, 0.876; total-pressure recovery, 0.985; total-pressure distortion parameter, D_{max}, 0.146; circumferential total-pressure distortion parameter, D_{60}, 0.021. (Data points G in figs. 8(d) and 9(d).)

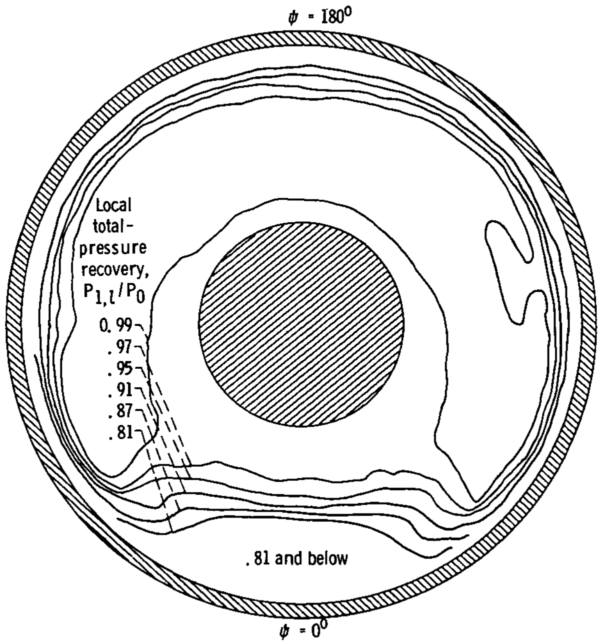

(c) Incidence angle, 50°; average throat Mach number, 1.0; total-pressure recovery, 0.942; total-pressure distortion parameter, D_{max}, 0.395; circumferential total-pressure distortion parameter, D_{60}, 0.12. (Data points H in figs. 8(d) and 9(d).)

Figure 11. - Total-pressure contours at rake measuring plane for translating-centerbody inlet in choked operating mode (centerbody extended). Free-stream velocity, 45 meters per second; corrected fan speed, $N/\sqrt{\theta}$, 34 700 rpm.

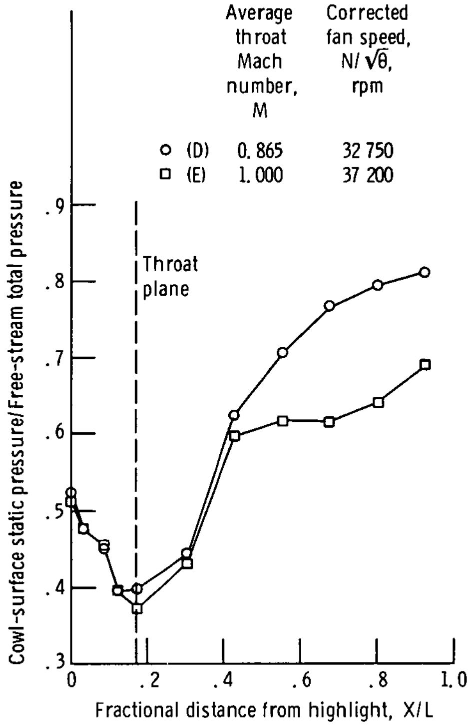

Figure 12. - Effect of average throat Mach number on axial variation of surface pressure ratio for a translating-centerbody inlet in choked operating mode (centerbody extended). Free-stream velocity, zero.

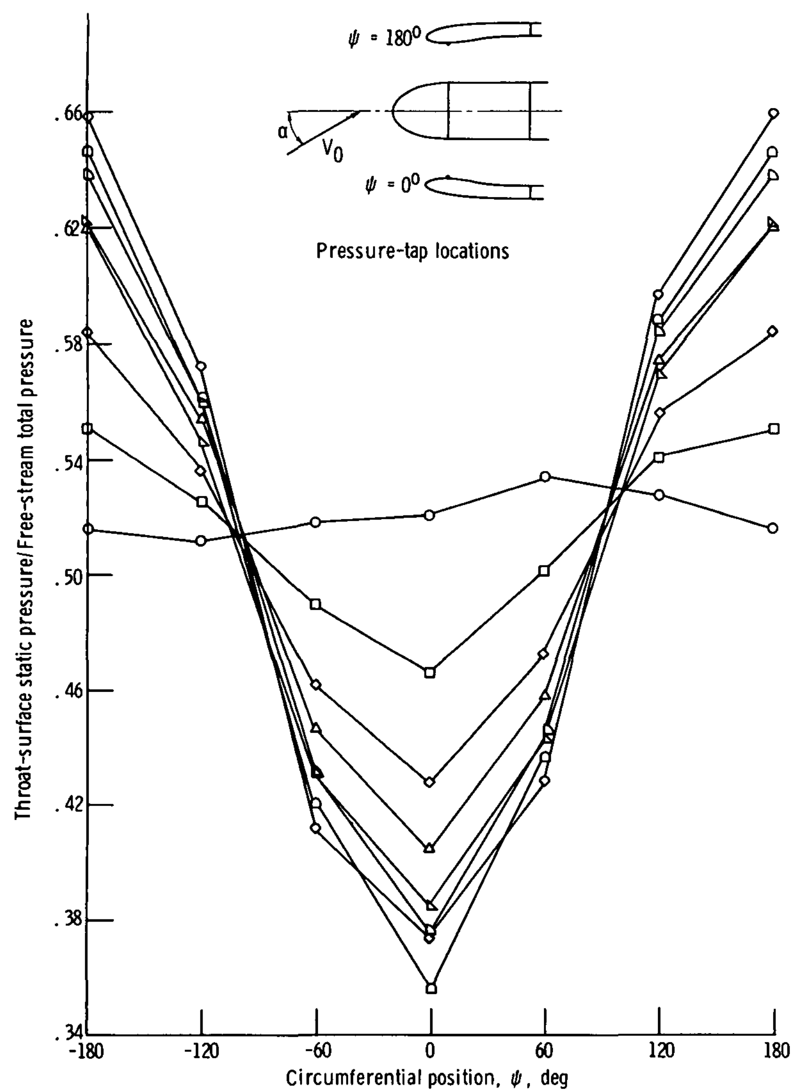

(a) Circumferential variation of surface pressure ratio at throat for low average throat Mach numbers. Corrected fan speed, $N/\sqrt{\theta}$, 32 500 rpm.

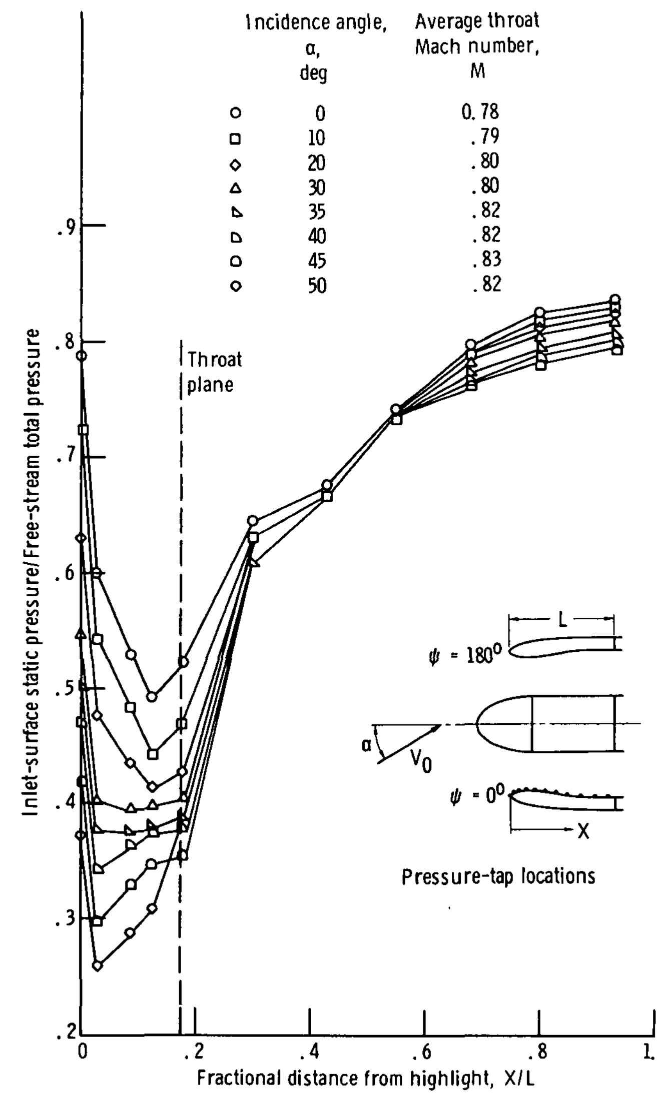

(b) Axial variation of surface pressure ratio at circumferential position $\psi = 0^0$ for low average throat Mach numbers. Corrected fan speed, $N/\sqrt{\theta}$, 32 500 rpm.

Figure 13. - Effect of incidence angle on surface static pressure distribution for translating-centerbody inlet in choked operating mode (centerbody extended). Free-stream velocity, 45 meters per second.

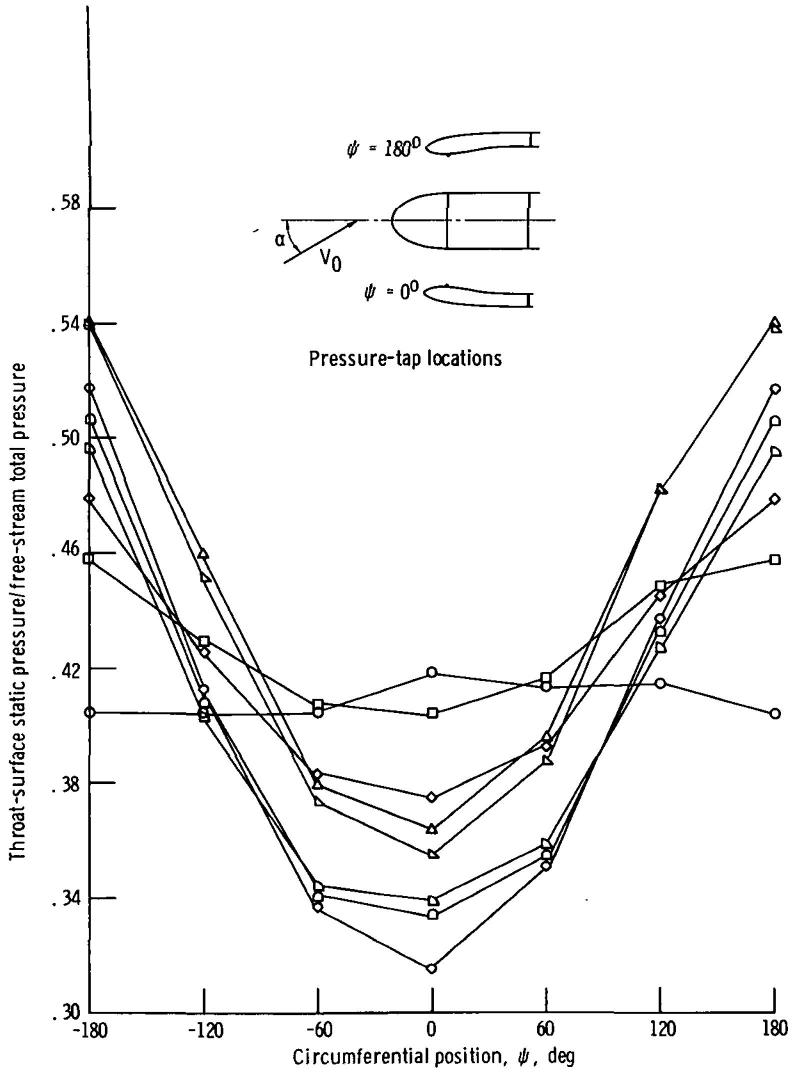

(c) Circumferential variation of surface pressure ratio at throat for high average throat Mach numbers. Corrected fan speed, $N/\sqrt{\theta}$, 34 700 rpm.

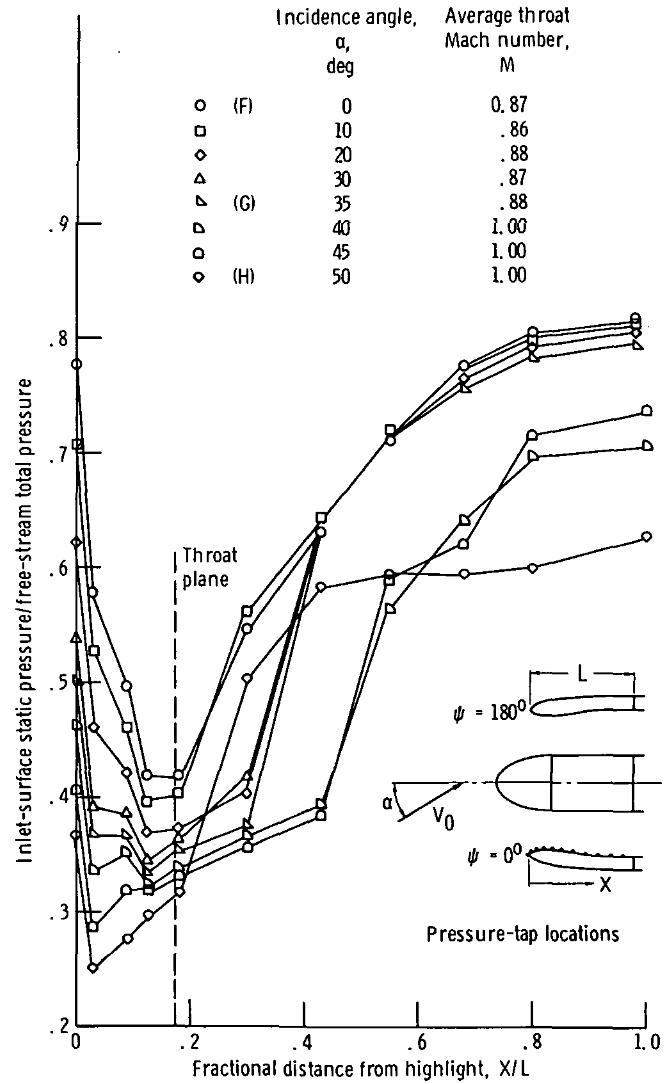

(d) Axial variation of surface pressure ratio at circumferential position $\psi = 0^0$ for high average throat Mach numbers. Corrected fan speed, $N/\sqrt{\theta}$, 34 700 rpm.

Figure 13. - Concluded.

	Incidence angle, α, deg	Average throat Mach number, M	Total-pressure recovery, P_1/P_0	Total-pressure distortion parameter, D_{max}	Circumferential total-pressure distortion parameter, D_{60}
○	(F) 0	0.87	0.988	0.075	0.0012
□	10	.86	.988	.092	.0043
◇	20	.88	.986	.118	.0110
△	30	.87	.986	.133	.0150
◺	(G) 35	.88	.985	.146	.0210
▷	40	1.00	.946	.270	.0410
▭	45	1.00	.949	.311	.0500
◇	(H) 50	1.00	.942	.395	.1200

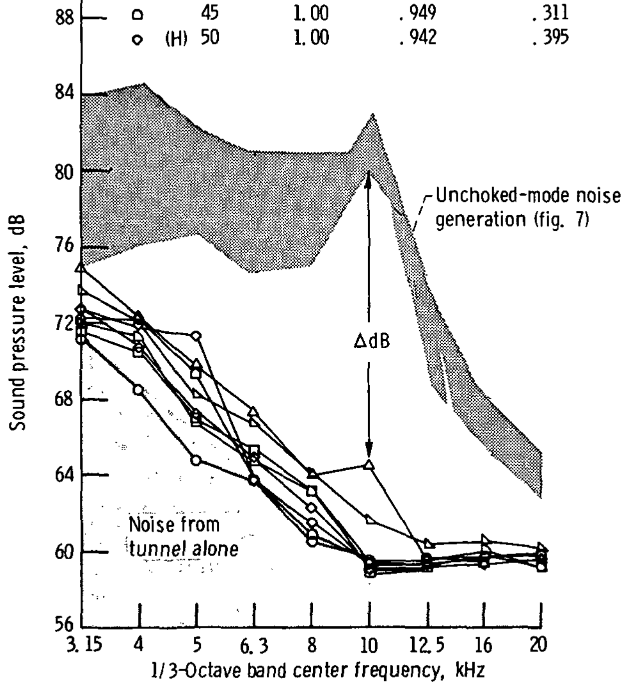

Figure 14. - Effect of incidence angle on noise generation of a translating-centerbody inlet in choked operating mode (centerbody extended). Free-stream velocity, 45 meters per second; corrected fan speed, $N/\sqrt{\theta}$, 34 700 rpm.

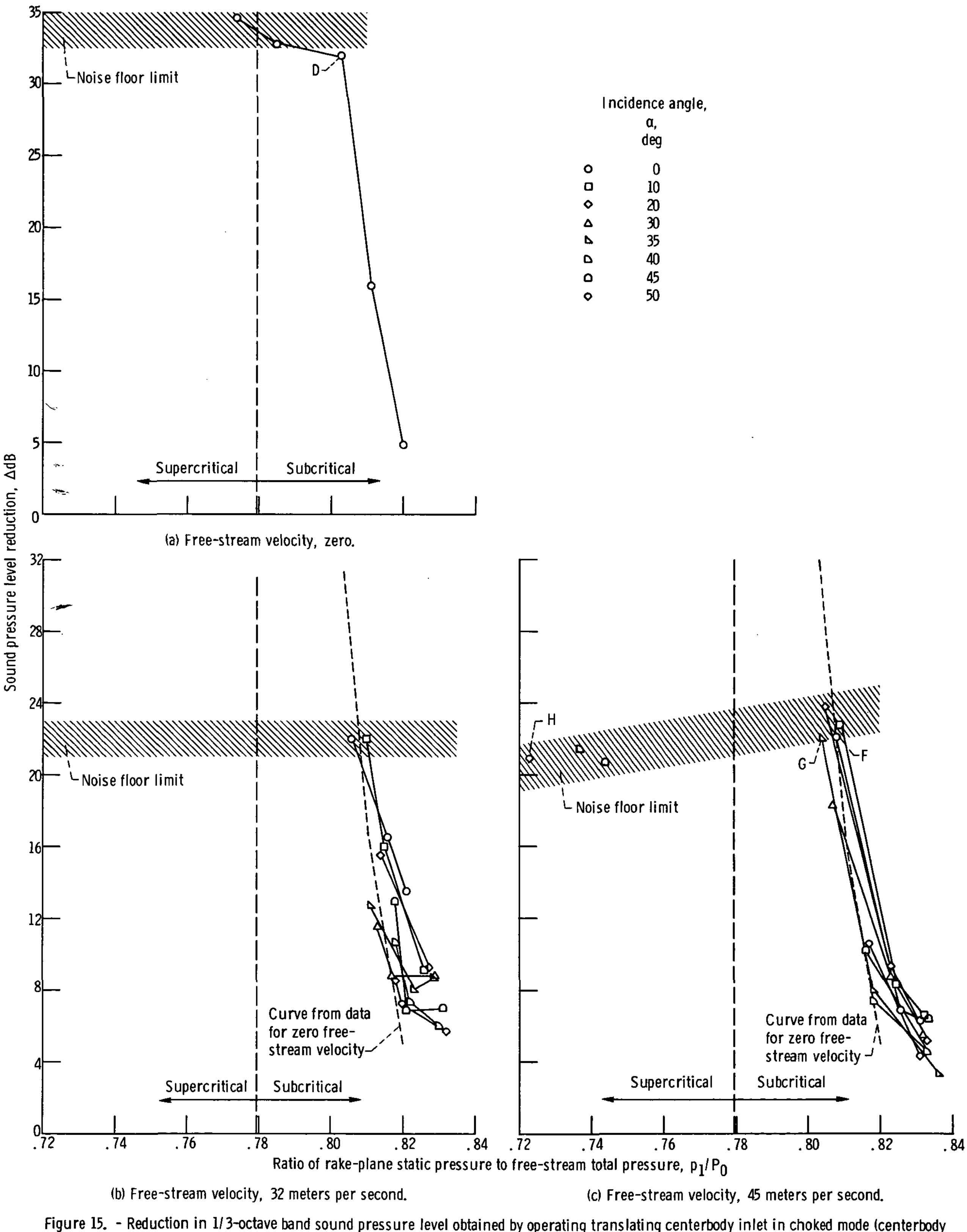

(b) Free-stream velocity, 32 meters per second.

(c) Free-stream velocity, 45 meters per second.

Figure 15. - Reduction in 1/3-octave band sound pressure level obtained by operating translating centerbody inlet in choked mode (centerbody extended). Corrected fan speed, $N/\sqrt{\theta}$, 30 000 to 35 000 rpm.

"The aeronautical and space activities of the United States shall be conducted so as to contribute . . . to the expansion of human knowledge of phenomena in the atmosphere and space. The Administration shall provide for the widest practicable and appropriate dissemination of information concerning its activities and the results thereof."

—NATIONAL AERONAUTICS AND SPACE ACT OF 1958

NASA SCIENTIFIC AND TECHNICAL PUBLICATIONS

TECHNICAL REPORTS: Scientific and technical information considered important, complete, and a lasting contribution to existing knowledge.

TECHNICAL NOTES: Information less broad in scope but nevertheless of importance as a contribution to existing knowledge.

TECHNICAL MEMORANDUMS: Information receiving limited distribution because of preliminary data, security classification, or other reasons. Also includes conference proceedings with either limited or unlimited distribution.

CONTRACTOR REPORTS: Scientific and technical information generated under a NASA contract or grant and considered an important contribution to existing knowledge.

TECHNICAL TRANSLATIONS: Information published in a foreign language considered to merit NASA distribution in English.

SPECIAL PUBLICATIONS: Information derived from or of value to NASA activities. Publications include final reports of major projects, monographs, data compilations, handbooks, sourcebooks, and special bibliographies.

TECHNOLOGY UTILIZATION PUBLICATIONS: Information on technology used by NASA that may be of particular interest in commercial and other non-aerospace applications. Publications include Tech Briefs, Technology Utilization Reports and Technology Surveys.

Details on the availability of these publications may be obtained from:

SCIENTIFIC AND TECHNICAL INFORMATION OFFICE

NATIONAL AERONAUTICS AND SPACE ADMINISTRATION

Washington, D.C. 20546